PHYSICAL MODELLING OF THE BOILING CRISIS: THEORY AND EXPERIMENT

Modélisation physique de la crise d'ébullition : théorie et expérience

Vadim Nikolayev[1,2*], **Denis Chatain**[1], **Daniel Beysens**[1,2]

[1] ESEME/SBT/INAC/CEA, 17 rue des Martyrs, 38054 Grenoble Cedex 9, France

[2]ESEME/PMMH/ESPCI, 10 rue Vauquelin, 75231 Paris Cedex 05, France

vadim.nikolayev@espci.fr, daniel.beysens@espci.fr, denis.chatain@cea.fr

In this presentation we describe a physical approach to the boiling crisis ("departure from nucleate boiling"). This approach is based on the hypothesis that the boiling crisis is triggered by spreading of individual vapor bubbles over the heater or equivalently by growth of dry spots under the bubbles. The role of bubble coalescence is assumed to be secondary. The spreading is due to forces acting at the microscopic scale, in the neighborhood of the line of triple contact of liquid, vapor and heater where the local heat fluxes are the strongest. This picture is supposed to be independent on boiling conditions. It is confirmed by the pool boiling experiments carried out at high pressure close to the critical pressure. Such unusual conditions are chosen to slow down the bubble growth sufficiently to be able to observe the dryout dynamics. In these experiments it lasted during about a minute. To keep the usual bubble geometry, it is necessary to perform such experiments under reduced gravity. Numerical simulations are carried out for high pressures. They show two regimes of bubble growth. When the heat flux is smaller than a threshold value associated with the CHF, a vapor bubble grows and then leaves the heater by buoyancy. When the heat flux is larger than the CHF, the bubble spreads over the heater without leaving it, in agreement with the experimental data. This occurs because the vapor recoil force causes both bubble spreading and its strong adhesion to the heater. The CHF variation with gravity is discussed.

I INTRODUCTION

When during boiling, the heat flux q from the heater exceeds a critical value (the Critical Heat Flux, CHF) the vapor bubbles on the heating surface form abruptly a film that thermally insulates the heater from the liquid. The heat transfer is blocked and the temperature of the heater rapidly grows. This phenomenon is known under the names of "boiling crisis" (BC) and "departure from nucleate boiling". Because the boiling crisis is very rapid under usual conditions, the correct CHF estimation requires a clear understanding of the physical phenomenon that triggers it. Among several dozens of existing models of BC (see [1, 2] for their discussion and classification), the classical Zuber model [3, 4] is the only one that can be considered as a theory, the others being mainly empirical or semi-empirical. According to this model, vapor columns form at the nucleation sites on the heater. The vapor moves upwards while the liquid moves to the bottom of the column where evaporation occurs. This counter-flow motion induces the Kelvin-Helmholtz instability, which is supposed to cause destabilization of the whole system and formation of a vapor film on the heater. This transition occurs when the vapor velocity exceeds a threshold [4] resulting in the following CHF (Zuber-Kutateladze) expression,

$$q_{CHF} \sim H[\sigma g(\rho_L - \rho_V)\rho_V^2]^{1/4}, \tag{1}$$

where H is the latent heat, ρ_L (ρ_V) is the density of the liquid (gas) phase, σ is the surface tension, and g is the gravity acceleration. While this expression fits a number of experimental data sets, the underlying physics is questionable. Indeed, the vapor column morphology of boiling is quite rarely observed while the BC occurs inevitably for all morphologies of boiling, for pool as well as for flow boiling. Besides, many experimental results, in particular those obtained in low gravity [5], cannot be fitted by Eq. (1). Other physical phenomena should then be responsible for the triggering of BC. A strong dependence of CHF on the wetting properties and the surface state of the heater [3] suggests a phenomenon at the level of the triple (vapor-liquid-solid) contact line rather than a phenomenon related to the bulk hydrodynamics.

*Corresponding author

There are two possible scenarios for the boiling crisis triggering. Either the dry spots under individual vapor bubble begin to grow independently and coalesce later or many neighboring bubbles begin to coalesce thus creating a growing dry spot. A thorough analysis [6] of this second scenario has shown a necessity of the repetitive (at least 30 – 40 times) formation of aggregates of 2 – 3 coalesced bubbles at the same neighboring nucleation spots. This is not a likely event because in order to coalesce, (i) the bubbles need to grow close to each other, which is prohibited by their thermal interaction [7, 8], and (ii) the strong lubrication forces between their interfaces need to be overcome [9], which means that either the bubble are densely crowded or strongly pinned at their nucleation sites. In the present paper we develop the first scenario that has been suggested initially by observation of growth of individual dry spots through the transparent heater [10, 11].

The dry spot growth will be discussed qualitatively in the next section. A numerical calculation of the CHF will be introduced next and some CHF results will be discussed. Finally, experimental observations will be discussed.

II WHY DOES THE DRY SPOT CAN GROW?

Consider a vapor bubble growing attached to a heater and surrounded by the liquid (Fig. 1). It is evident that the fast (on the timescale of bubble residence) increase of the dry spot means that the bubble spreads along the heater. Such quick bubble spreading can be explained by the effect of the vapor recoil force, a force coming from the uncompensated mechanical momentum of the fluid molecules that leave the vapor-liquid interface. One finds that the vapor recoil force per interface area is [12]

$$P_r = \eta^2(\rho_V^{-1} - \rho_L^{-1}). \tag{2}$$

Here η is the mass evaporation rate [kg m^{-2} s^{-1}] per unit area of the liquid-vapor interface. It is related to the local heat flux q_L (taken at the liquid side of the interface) by the equality

$$q_L = H\eta, \tag{3}$$

where the heat conduction in the vapor is neglected with respect to that in the liquid.

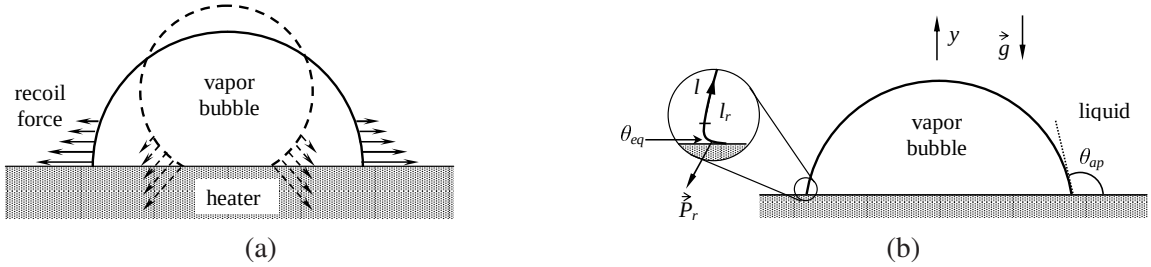

Figure 1 : Vapor bubble at the heater. (a) Sketch illustrating how the vapor recoil initiates the bubble spreading. The amplitude and direction of the vapor recoil force are shown by arrows. The thickness of the area where the vapor recoil is important (i.e. of the microregion) is exaggerated. (b) Sketch showing the difference between the actual (θ_{eq}) and apparent (θ_{ap}) contact angles. The curvilinear coordinate l varying along the bubble contour is shown. The microregion $0 < l < l_r$ corresponds to the interface area where the contour curvature varies strongly. The directions of gravity and ordinate axis are shown.

The evaporation is particularly strong inside the superheated layer of liquid adjacent to the heater. During the bubble growth this layer is usually thin with respect to the bubble size. The vapor recoil force is thus strongly localized in the vicinity of the contact line of the bubble, in the area called often microregion. This region is to be distinguished from the macroregion, the rest of the liquid domain. The recoil force creates simultaneously two effects. First, its horizontal component can pull apart the bubble contact line and make the bubble spread over the heater. Second, its vertical component is directed downwards and creates an additional bubble adhesion force. The first effect tends to create a nucleus for the vapor film. The second provides a sufficient time for the spreading by keeping the bubble at the heater.

As sketched in Fig. 1a, the bubble spreading means the increase of the apparent contact angle θ_{ap} (measured from the liquid side). This increase is the result of the strong interface curvature K encountered in the microregion (Fig. 1b) during evaporation. By definition, a large K means a quick change of the bubble contour slope with l. The quick change of the slope near the contact line means large difference of the actual θ_{eq} and apparent contact angles (Fig. 1b). The large K value appears because of strong localization of the evaporation in the microregion and is due to two main physical effects: the viscous pressure drop and the vapor recoil force. In the liquid wedge, the pressure drop is high because the evaporation attains its maximum at the contact line [13]. The flow toward the contact line is needed to supply it with the liquid. Since the cross-section of the wedge decays near the contact line, both the fluid velocity and the viscous stresses increase. Since the interface is free, the Laplace pressure σK needs to compensate the normal viscous stress so that the wedge becomes more and more concave when the contact line is approached as sketched in Fig. 1b. The pressure drop is proportional to the evaporation rate η [13].

The vapor recoil also leads to high curvature (see section IV). The only difference is that the corresponding pressure contribution (2) is proportional to η^2. Therefore the effect of the viscous pressure drop prevails at small heat fluxes while the vapor recoil effect should be dominant near the CHF.

Bubble spreading does not allow alone to calculate q_{CHF}. The bubble residence time is also important. At $q < q_{CHF}$, the bubble leaves the heater under the action of buoyancy or other forces before the spreading could start. At $q \geq q_{CHF}$ the bubble spreading occurs. It is accompanied by a local increase of the heater temperature that causes a still larger local increase of evaporation and thus of the vapor recoil. The latter not only accelerates the spreading but also creates a strong adhesion of the bubble to the heater. The bubble can thus keep spreading until it coalesces with the neighboring spreading bubbles. The CHF can be therefore defined as a threshold flux separating the regimes of bubble departure and bubble spreading.

III VAPOR RECOIL AND ZUBER-KUTATELADZE FORMULA

A rough estimation of the CHF can be performed with the vapor recoil initiating the bubble spreading when its effect becomes comparable with that of the surface tension. This condition can be written by the scaling relation

$$\int_0^w P_r \mathrm{d}l \sim \sigma \tag{4}$$

that should be valid at the moment of bubble departure and for $q = q_{CHF}$. Here w is the bubble contour half-length. One can use the proportionality $q_L \sim q$. As mentioned above, the vapor recoil is localized in the narrow band $0 < l < l_r$ and the integral can thus be replaced by the product $P_r l_r$. The length l_r scales as the bubble radius, which is at bubble departure is of the order of the capillary length $l_c = \sqrt{\sigma/g(\rho_L - \rho_V)}$. Note that by using this consideration, one neglects the influence of the vapor recoil on the bubble departure conditions. Finally, one obtains from (4) the CHF expression

$$q_{CHF} \sim H \left(\frac{\sigma g \rho_V^2 \rho_L^2}{\rho_L - \rho_V} \right)^{1/4}. \tag{5}$$

One can notice that at small pressures $\rho_L \gg \rho_V$ and the expressions (1) and (5) coincide. It means that at low pressures the vapor recoil mechanism and the Zuber-Kutateladze formula should result in the similar CHF values. High pressure experiments (see below) are thus needed to distinguish these mechanisms. It is clear that the criterion (5) needs to be treated with caution because important simplifications were made during its derivation.

IV BOILING CRISIS NUMERICAL SIMULATION

The physical model and the mathematical formulation is similar to that of [14] and differs only by the account of the gravity g that enters the equation defining the bubble shape

$$K\sigma = \Delta p + P_r + gy(\rho_L - \rho_V), \tag{6}$$

where y is the ordinate (see Fig. 1b) and Δp is the pressure jump at the vapor-liquid interface. This equation holds for the thermally controlled (slow) bubble growth where the hydrodynamic inertial forces are negligible. This approximation is justified for the high pressure experiments described in the next section. Following the reasoning of the previous section, we neglect the viscous pressure drop with respect to the vapor recoil contribution. It means that the pressure jump is independent of l, which corresponds to the quasi-static approximation for the bubble shape. Δp defines the averaged bubble curvature (i.e. its size) and can be calculated when the bubble volume V is known. V is given by the usual for the thermally controlled growth equation

$$H\rho_V \frac{\mathrm{d}V}{\mathrm{d}t} = 2\int_0^w q_L \,\mathrm{d}l, \tag{7}$$

where t is the time. Note that Eq. (6) is a second order differential equation because K contains the second derivative of the function that defines the (free) bubble interface.

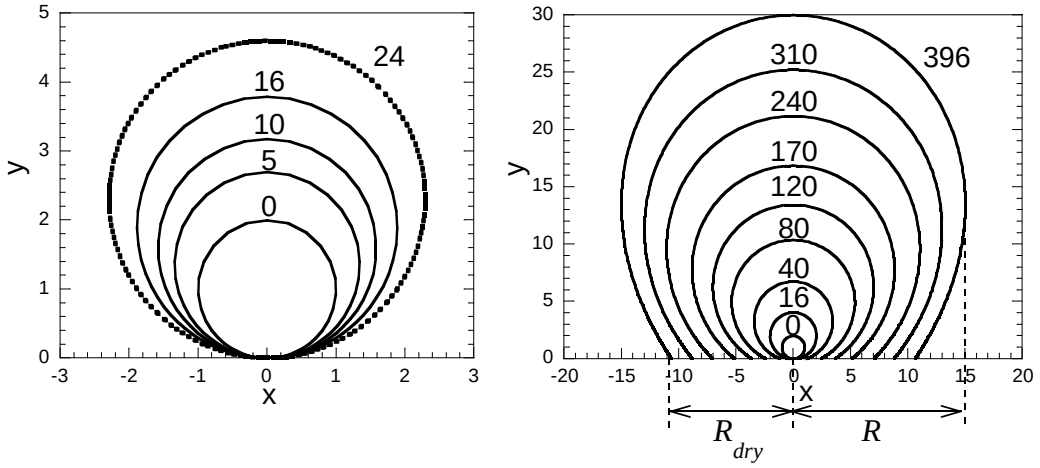

(a) (b)

Figure 2 : Simulations of the bubble growth for $g = g_0$ (Earth gravity) and $\theta_{eq} = 0.5°$. $q_{CHF} = 0.144\,\mathrm{W\,cm^{-2}}$. The parameters of the curves are the growth times in ms. The co-ordinate values are relative to the initial bubble radius ($= 50\,\mu$m). (a) Regime of bubble departure, $q = 0.142\,\mathrm{W\,cm^{-2}} < q_{CHF}$; the dotted contour corresponds to the moment of bubble departure. (b) Regime of bubble spreading, $q = 0.16\,\mathrm{W\,cm^{-2}} > q_{CHF}$.

The heat conduction problem is solved in the liquid and in the solid in order to determine $q_L = q_L(l,t)$. Unlike [13], the simulation domain is treated uniformly, without cutting it into micro and macro regions. A high resolution in the microregion is attained by a high density of the mesh in this region. The mesh spatial step attains there 10^{-4} of the bubble diameter. The gravitational convection is neglected.

The temporal evolution of the bubble in 2D is presented in Fig. 2a for the regime of bubble departure and in Fig. 2b for the regime of bubble spreading. Calculation is carried out for water at 10 MPa and the stainless heater as in [14].

The difference between the two regimes is evident in Fig. 3a where the temporal evolution of the ratio of the dry spot radius R_{dry} to the visible bubble radius R (see Fig. 2b for their definitions) is presented. At small q values, the dry spot increases slightly before decaying to zero where the bubble departure occurs. At large heat flux, the dry spot increases abruptly after a period of slow growth. One notices the sharpness of the transition between the two regimes.

The numerical algorithm is modified considerably compared to that used in [14]. Numerical instabilities which were at the origin of the oscillations of the $R_{dry}(t)$ curve have disappeared. The precision of the determination of the beginning of the bubble spreading and thus the precision of the CHF determination are largely improved.

The CHF determined as described above can be plotted as a function of the gravity level (Fig. 3b). The growth of the CHF with gravity is in qualitative agreement with the reduced gravity experiments [5]. The deviation of

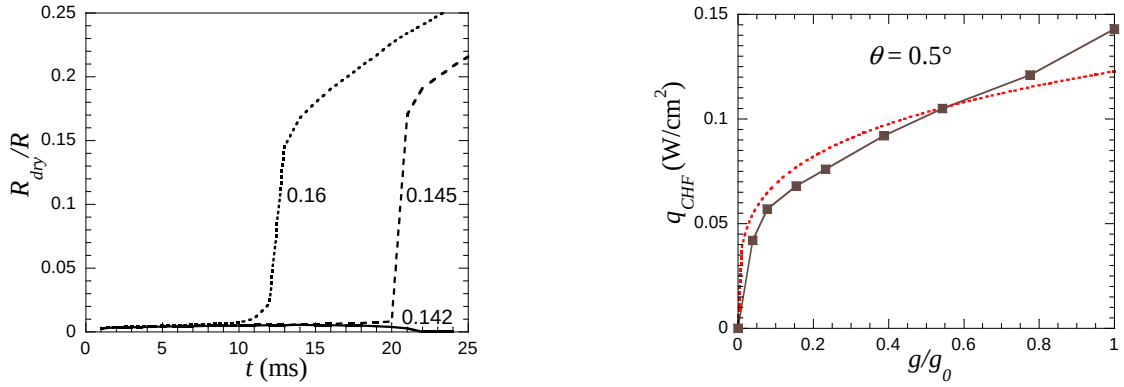

Figure 3 : (a) Evolution of the dry spot for $g = g_0$ and $\theta_{eq} = 0.5°$. The parameters of the curves are the values of q in W cm^{-2}. From these curves one establishes that CHF is between 0.142 and 0.145 W cm^{-2}. (b) Calculation of the CHF versus the level of gravity for $\theta_{eq} = 0.5°$ (squares and solid line). The dotted line is the power $1/4$ fit that ought to be valid according to the Zuber-Kutateladze expression (1) and simplified model result (5).

the data from the fit to the expression (5) is the result of the simplifications made during its derivation. For low g, the CHF increases abruptly for $g < 0.07 g_0$; then its growth decelerates.

The calculated value of the CHF is several times smaller than the experimental values. This difference can be attributed to the assumption of constant temperature (equal to T_{sat} corresponding to the system pressure) of the interface liquid-vapor. In reality, the interface temperature is higher in the microregion, mostly because of the strongly varying local pressure [13] (see the viscous pressure drop discussion above). We thus overestimate q_L and P_r, which results in the underestimation of the CHF. A more sophisticated model of the microregion has to be used in the future simulations.

V EXPERIMENTS

We describe here the observations made at high pressure, in the vicinity of the liquid-gas critical point. The bubble growth is very slow there because the thermal diffusivity is very small. This permits to observe the very dynamics of BC which is usually extremely fast (at low pressures). The turbulence of the liquid, which obstructs the optical observation, is avoided. The CHF is known to become very small near the critical point and optical aberrations related to the temperature gradients are absent. However the capillary length l_c strongly decreases because of the weak surface tension. The gravity flattens the liquid-vapor interface. To keep a convex shape of the bubbles, the gravity should be reduced. A cryogenic facility [15] is used to compensate the gravity by magnetic forces in hydrogen (critical temperature $T_c = 33$K). Since the magnetic force acting on non-magnetic substances (H_2 is diamagnetic) acts on each atom, the force per unit volume is proportional to the fluid density, just like the weight. It means that if the compensation is attained for the liquid phase, it is attained for the vapor too.

The fluid cell is a (closed) cylinder of 8 mm diameter and 5 mm thickness (Fig. 4). The best observations of BC [4, 10, 11, 16, 17] involve a transparent heater to detect and follow the heater dryout. The flat pieces of our cell are the observation windows made of transparent sapphire that is also an excellent thermal conductor. The lateral cell wall is made of stainless steel, with conductivity about 10^3 times less than that of the sapphire. The cell is placed in vacuum inside an "anti-cryostat", which is in its turn situated inside a cryostat that contains liquid He. Several thermistors are integrated into two copper rings ("bases") that have a good thermal contact with the windows. Both bases are connected thermally to a colder liquid helium bath with wires that serve as thermal resistances. The thermistors are used to inject a controlled heat power into the windows. One of them is used as a heater, the temperature T of which is measured with a thermistor. The temperature of the other is maintained at T_{sat} by a system of temperature regulation that controls the corresponding thermistors. This system also enables the measurement of the extracted heat and thus of the heat flux q emitted by the heater.

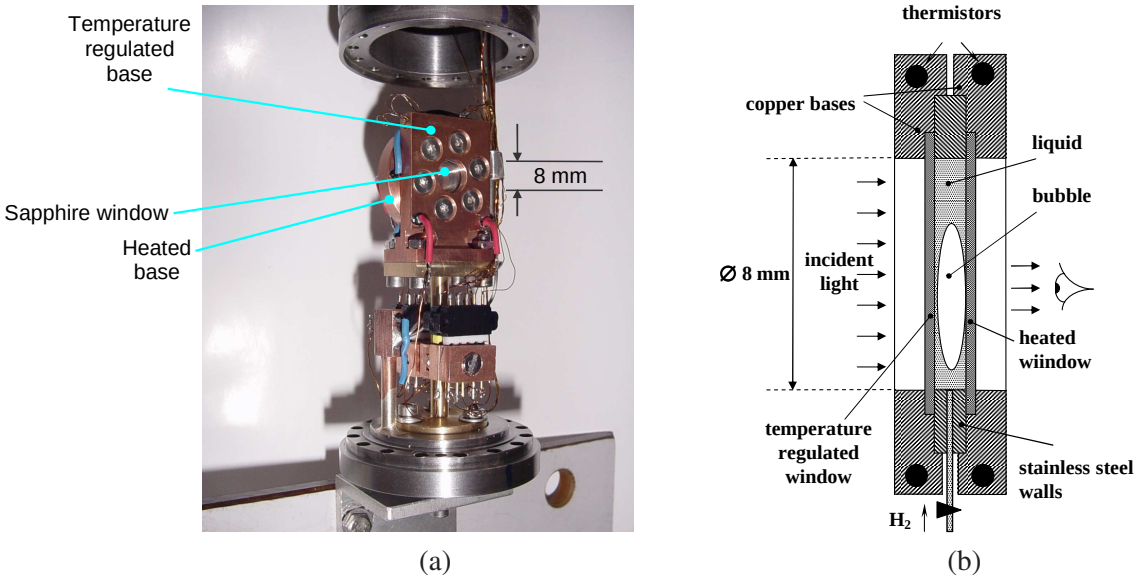

Figure 4 : H_2 boiling cell. (a) Photo. (b) Sketch of the cell (cross-section).

The fluid evaporated on the heating window recondenses at the other window and the pressure remains constant. The boiling curve $q(T - T_{sat})$ is measured simultaneously with optical observations. They show a conventional N shape, which permits to determine precisely the CHF as a function of T_{sat}, i.e. of the fluid pressure. It is important to note that these measurements are found [18] to be in a good quantitative agreement with the scaling relations predicted by some of us [19] in the framework of the vapor recoil model of BC.

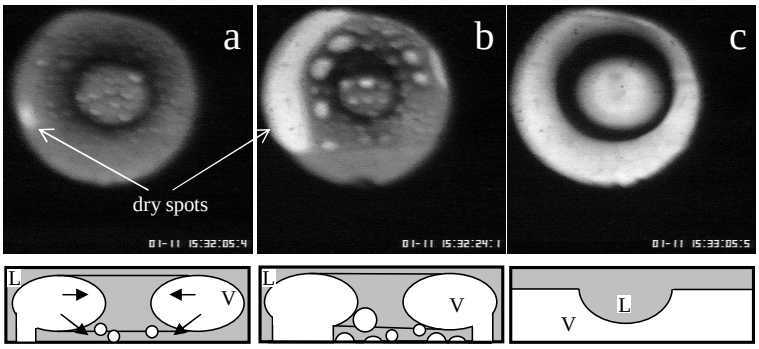

Figure 5 : Heater drying dynamics at the CHF at $T_{sat} = T_c - 50$mK (the large bubble has a toroidal shape as described in the text) visualized through the transparent heater (closest to the observer). The section of the cell interior with a plane perpendicular to the image is sketched below the corresponding photo. On the sketches, the vapor is white and the liquid is gray; the heater is at the bottom. The bright areas on the photos are the dry spots. (a) Beginning of the dry spot (small white spot to the left) growth. (b) Intermediate stage. (c) Complete drying of the heater; the liquid phase has taken a shape of a hat turned upside down. Nucleated small bubbles are visible in (a-b). The direction and the relative magnitude of the effective gravity are shown by arrows in the sketch (a).

The cell can be partially filled or pumped off *in situ* by using a capillary equipped with a cryogenic electric valve. The latter remains closed during the experiment. The cell is filled with H_2 at critical density ρ_c so that the gas phase occupies a half of the cell independently of T because of the symmetry of the co-existence curve with respect to ρ_c: $(\rho_L + \rho_V)/2 = \rho_c$. During the evolution, the bubble mass grows while its volume does not change.

Because of the complete wetting conditions characteristic of near critical fluids [19], the wetting layer always covers the cell interior at equilibrium. Due to this fact, a good thermal contact of the temperature controlled window with the rest of the fluid is provided. The cell location with respect to the magnetic field is chosen in such a way that the residual magnetic force (which plays the role of the gravity $\approx 0.02 g_0$) positions the bubble

against the heating plate. This effective gravity field is directed towards the cell center ([15], see the sketch in Fig. 5a) so that the denser liquid phase is attracted to the cell center. Unfortunately, it is quite difficult to quantify the actual force acting on the bubble since there is no possibility to map the magnetic field with the sufficient precision.

The surface tension prevents the liquid from gathering in the cell center by keeping the bubble convex, and the bubble image is circular far from T_c. Close to the critical point, the surface tension becomes too weak and the liquid gathers in the center. Since the wetting layer remains at the cell walls, the bubble takes an unusual torus shape, see Fig. 5. This occurs for $T_{sat} \geq T_c - 100$mK.

The dynamics of the heater temperature is interesting. At the CHF, the BC does not occur immediately after the heating starts. T first attains a metastable state where it fluctuates slightly. One of the fluctuations leads to a rapid drying of the major part of the heater. Then the liquid loses completely its contact with the heater and the transferred heat flux q falls sharply. No fluid motion is observed any more since the heat is transferred through the cylindrical walls of the cell rather than through the fluid. No interface instability characteristic of the film boiling occurs because the residual gravity is too weak.

The optical observations of the boiling dynamics show that when q is close to the CHF the dry spots under the bubbles appear and disappear later, when the bubbles depart from the heater. A bubble that appears in the hottest point coalesces with the toroidal bubble and forms a dry "bridge" which appear and disappear intermittently. At $q = q_{CHF}$ a large dry spot appears (Fig. 5a) and keeps growing (Fig. 5b). Smaller dry spots under other bubbles keep appearing and disappearing but grow larger. All the dry spots finally grow so large that they coalesce and, suddenly, the heater dries out completely (Fig. 5c). This picture is in agreement with the observations [16, 17] performed at much lower pressures. As expected, the BC slows down near T_c, and can take as long as 1-2 min for the closest to T_c runs.

VI CONCLUSIONS

A self-consistent model of the BC has been developed. It shows that the BC is triggered by the spreading of individual vapor bubbles due to the action of the vapor recoil. The CHF value can be determined as a threshold between bubble departure and bubble spreading regimes. It is shown that such an approach results in an approximate CHF expression similar to that of Zuber and Kutateladze. To obtain the numerical CHF values, a simulation of growth of a single vapor bubble is however required. Capturing the vapor recoil effect requires an extremely delicate treatment of the heat flux maximum in the vicinity of the triple vapor-liquid-heater contact line need to be performed. The CHF is calculated as a function of gravity within an approach where the liquid-vapor interface is assumed to be isothermal even in the vicinity of the contact line. A more refined approach is needed to gain a quantitative agreement with the experiment. The experiments at nearly critical pressure can give very detailed information about the CHF due to the small CHF value and the slowness of the bubble growth. Reduced gravity conditions were required to observe the bubbles. During the BC, we observed clearly the growth of individual dry spots under the bubbles prior to their coalescence, in agreement with the theoretical and numerical predictions. The behavior of the CHF as a function of pressure near the critical pressure is in quantitative agreement with the predictions of the vapor recoil model of bubble spreading.

ACKNOWLEDGMENT

A financial support of CNES is gratefully acknowledged.

REFERENCES

[1] Brusstar, M. J., H. Merte, J., Keller, R. B., & Kirby, B. J. (1997). – Effects of heater surface orientation on the critical heat flux–I. An experimental evaluation of models for subcooled pool boiling. *Int. J. Heat Mass Transfer*, **40**, 4007 – 4019.

[2] Buyevich, Y. A. (1999). – Towards a unified theory of pool boiling – the case of ideally smooth heated wall. *Int. J. Fluid Mech. Res.*, **26**, 189 – 223.

[3] Dhir, V. (1998). – Boiling heat transfer. *Ann. Rev. Fluid Mech.*, **30**, 365 – 401.

[4] Theophanous, T. G., Dinh, T. H., Tu, J. P., & Dinh, A. P. (2002). – The boiling crisis phenomenon. Part II: Dryout dynamics and burnout. *Exp. Thermal Fluid Sci.*, **26**, 793 – 810.

[5] Marek, R. & Straub, J. (2001). – The origin of thermocapillary convection in subcooled nucleate pool boiling. *Int. J. Heat Mass Transfer*, **44**, 619 – 632.

[6] Bricard, P., Péturaud, P., & Delhaye, J.-M. (1997). – Understanding and modeling DNB in forced convective boiling: Modeling of a mechanism based on nucleation site dryout. *Multiphase Sci. Techn.*, **9**, 329 – 379.

[7] Kenning, D. B. R. & Valle, V. H. D. (1981). – Fully-developed nucleate boiling: Overlap of areas of influence and interference between bubble sites. *Int. J. Heat Mass Transfer*, **24**, 1025 – 1032.

[8] Pasamehmetoglu, K. O. & Nelson, R. A. (1991). – Cavity-to-cavity interaction in nucleate boiling: the effect of heat conduction within the heater. *AIChE Symp. Ser.*, **87**, 342 – 351.

[9] Yiantsios, S. G. & Davis, R. H. (1991). – Close approach and deformation of two viscous drops due to gravity and van der Waals forces. *J. Colloid Interface Sci.*, **144**, 412 – 433.

[10] van Ouwerkerk, H. J. (1972). – Burnout in pool boiling: the stability of boiling mechanisms. *Int. J. Heat Mass Transfer*, **15**, 25 – 34.

[11] Torikai, K., Suzuki, K., & Yamaguchi, M. (1991). – Study on contact area of pool boiling bubbles on a heating surface. *JSME Int. J. Series II*, **34**, 195 – 199.

[12] Nikolayev, V. S. & Beysens, D. A. (1999). – Boiling crisis and non-equilibrium drying transition. *Europhysics Lett.*, **47**, 345 – 351.

[13] Stephan, P. & Hammer, J. (1985). – A new model for nucleate boiling heat transfer. *Wärme- und Stoffübertrangung*, **30**, 119 – 125.

[14] Nikolayev, V. S., Beysens, D. A., Lagier, G.-L., & Hegseth, J. (2001). – Growth of a dry spot under a vapor bubble at high heat flux and high pressure. *Int. J. Heat Mass Transfer*, **44**, 3499 – 3511.

[15] Chatain, D. & Nikolayev, V. S. (2002). – Using magnetic levitation to produce cryogenic targets for inertial fusion energy: experiment and theory. *Cryogenics*, **42**, 253 – 261.

[16] Kandlikar, S. G. & Steinke, M. E. (2002). – Contact angles and interface behavior during rapid evaporation of liquid on a heated surface , , 2002. *Int. J. Heat Mass Transfer*, **45**, 3771 – 3780.

[17] Nishio, S. & Tanaka, H. (2004). – Visualization of boiling structures in high heat-flux pool-boiling. *Int. J. Heat Mass Transfer*, **47**, 4559 – 4568.

[18] Nikolayev, V. S., Chatain, D., Garrabos, Y., & Beysens, D. (2006). – Experimental evidence of the vapor recoil mechanism in the boiling crisis. *Phys. Rev. Lett.*, **97**, 184503.

[19] Garrabos, Y., Lecoutre-Chabot, C., Hegseth, J., Nikolayev, V. S., Beysens, D., & Delville, J.-P. (2001). – Gas spreading on a heated wall wetted by liquid. *Phys. Rev. E*, **64**, 051602.